CHAPTER 1: METHODS TO EXPLORE THE CELLULAR UPTAKE OF LUMINESCENT RUTHENIUM COMPLEXES[†]

1.1: INTRODUCTION

1.1.1: SIGNIFICANCE OF UPTAKE

Transitional metal complexes are appealing candidates in the search for new diagnostic and therapeutic agents. They represent a uniquely modular system, wherein the metal center holds its ligands in a precisely defined three-dimensional structure. These ligands can be varied relatively easily, in order to selectively change the characteristics of the complex in either subtle or dramatic fashion. Transition metal complexes also offer rich photophysical and photochemical properties, expanding their utility beyond structural recognition.

Biological applications of transition metal complexes are increasingly being explored.[1–3] Currently, we are investigating 5,6-chrysenequinone diimine (chrysi) complexes of rhodium(III) as potential chemotherapeutic agents. These complexes target single base mismatches in DNA and selectively inhibit cellular proliferation in mismatch repair-deficient cell lines.[4–6] To be effective, these compounds must reach the intended location inside the cell.

The cell membrane represents a formidable barrier to this goal. Only molecules within a narrow range of molecular weight, charge, and polarity are typically able to directly cross the plasma membrane by passive diffusion.[7] Larger molecules are generally

[†] Parts of this chapter were adapted from Puckett, C. A.; Barton, J. K. Methods to explore cellular uptake of ruthenium complexes. *J. Am. Chem. Soc.* **2007,** *129,* 46–47.

internalized by endocytosis, a process that involves invagination of the plasma membrane to form a vesicle. However, molecules that enter by this route often fail to escape from these vesicles. Compounds that target genomic DNA must also bypass the nuclear membrane.

The cellular uptake properties of transition metal complexes are not well developed. The notable exception is cisplatin, whose cellular accumulation has been examined in detail and recently reviewed.[8] Also, Parker and coworkers have characterized the mechanism of uptake for several luminescent Eu(III) and Tb(III) complexes, and found that they enter cells by endocytosis (specifically macropinocytosis).[9] Generally, studies of metallocomplexes have revealed that they are as diverse in their uptake properties as organic and biomolecular compounds. Here, we apply a broad spectrum of techniques to explore the uptake and distribution of ruthenium(II) polypyridyl complexes, which serve as luminescent analogues of our rhodium therapeutics.

1.1.2: METHODS TO EXAMINE CELLULAR ACCUMULATION OF METAL COMPLEXES

Metal complexes for diagnostic applications are frequently luminescent, allowing ready characterization of their uptake characteristics. They can be examined by fluorometry, confocal microscopy,[3] and flow cytometry.[10] For non-luminescent complexes, inductively coupled plasma mass spectrometry (ICP-MS),[11,12] atomic absorption spectroscopy (AAS),[13] and UV-visible absorption spectroscopy[14] are used.

Prior to ICP-MS, AAS, UV-visible absorption spectroscopy, and fluorometry

measurements, cell lysates are prepared from cells that have been incubated with metal complex. When adherent cells are used, they are either detached from the culture dish and then lysed, or lysed directly in the dish. Alternatively, the cells can be detached and treated with complex in suspension, though in this case, the cells are not in their normal growing environment. This cell lysate is analytically diluted, and the amount of metal in the solution is quantified. Amounts are typically reported versus cell number or total protein concentration. Independent of the quantification technique, attention must be paid to certain steps to ensure accurate results. Egger and colleagues have found that adsorption to the culture plates and sample storage conditions prior to analysis significantly influence recovery of the metal.[11] Factors affecting adsorption include concentration of the complex, the amount of protein in the medium, the duration of contact of protein-containing medium before treatment with complex, and the lipophilicity of the complex. Adsorption-related artifacts are particularly an issue when lysis is performed directly in the culture dishes. To correct for these effects, adsorption blanks of cell-free samples treated with metal complex should be performed. A second major issue is the time that the sample is stored prior to measurement, as the recovery of analyte decreases with time. Consequently, samples should be quantified immediately after preparation. When these considerations are taken into account, reliable measurements of metal complex uptake can be performed.

The cellular uptake of luminescent metal complexes are primarily examined using two complementary methods, flow cytometry and confocal microscopy; fluorometry of cell lysates can also be performed. For flow cytometry, cells are detached from culture

either before or after incubation with the metal complex to produce a cell suspension. Untreated cells are used for the autofluorescence control. To exclude dead cells from analysis, a membrane-impermeable dead cell dye, such as propidium iodide, can be added.[15] The cells are inspected individually as they pass single file through the laser beam(s) and the instrument records their light scatter and luminescence. Optical band pass filters separately collect the emission from multiple fluorophores. The result is a distribution of luminescence for the cell population, which can be depicted as a histogram of luminescence intensity versus the number of cells. The luminescence intensity of different cell populations, e.g., treated with different complexes or different incubation conditions, is easily compared.

Flow cytometry is faster and less labor intensive than preparation of samples for ICP-MS. It also provides a distribution of cellular uptake, rather than only the mean uptake of all the cells. Samples prepared for flow cytometry will have the same adsorption issues described above, though they may be less significant, as the cells are detached from the culture dish after incubation with the metal compound, rather than lysed in the dish, or incubated in suspension following detachment. Flow cytometry distinguishes live from dead cells by uptake of a dead cell dye, whereas with ICP-MS, dead cells are eliminated from analysis if they have lost adherence to the culture dish and are washed away before the lysis step. Both techniques have their purpose, as ICP-MS provides absolute values for uptake, while flow cytometry is limited to luminescent compounds and is better suited for comparing the amount of uptake under different conditions.

Flow cytometry and analysis of cell lysates by ICP-MS and other methods only provide a measurement of the total amount of metal complex associated with the cell; they do not distinguish between membrane-bound and intracellular material. Localization is difficult to discern by these techniques, where cellular components, such as nuclei, must be physically isolated before the metal content can be determined.

Confocal microscopy, on the other hand, reveals the spatial distribution of luminescent metal complexes inside the cell. Co-staining with organelle dyes can be performed to further pinpoint their intracellular location. Another notable advantage of microscopy over ICP-MS is that lesser amounts of metal complex are typically required, as the incubations can be performed in small wells (e.g., those of a 96-well plate). To acquire better quality images, adherent cells are preferable over suspension cells, and the cells should not be confluent. Importantly, cells should be imaged live rather than fixed, as fixation can cause artifactual redistribution of compounds.[16] In all the uptake experiments, attention should be paid to the number of cells incubated with the metal complex, since the amount of uptake may be dependent on it. This has been shown to be the case for cell-penetrating peptides.[17]

1.2: EXPERIMENTAL PROTOCOLS

1.2.1: MATERIALS AND INSTRUMENTATION

Media, cell culture supplements, and TO-PRO®-3 iodide were purchased from Invitrogen (Carlsbad, CA). $RuCl_3$ was purchased from Pressure Chemical Co (Pittsburgh, PA). 2,2′-bipyridine (bpy), 1,10-phenanthroline (phen), 4,4′-dimethyl-2,2′-bipyridine, and

3,4,7,8-tetramethyl-1,10-phenanthroline (Me_4phen) were obtained from Sigma-Aldrich (St. Louis, MO). 4,7-diphenyl-1,10-phenanthroline (DIP) was purchased from GFS Chemicals (Columbus, OH). Calf thymus (CT) DNA was purchased from Amersham Biosciences, GE Healthcare (Pittsburgh, PA). All commercial materials were used as received.

^{1}H NMR spectra were recorded on a 300 MHz Varian spectrometer. Mass spectrometry was performed at either the Caltech mass spectrometry facility or in the Beckman Institute Protein/Peptide Micro Analytical Laboratory. Absorption spectra were recorded on a Varian Cary 100 or Beckman DU 7400 spectrophotometer. Unless otherwise referenced, extinction coefficients of Ru complexes were determined using inductively coupled plasma mass spectrometry (ICP-MS). Luminescence measurements were performed on an ISS K2 fluorimeter equipped with a 300 W xenon lamp as an excitation source. HPLC was performed on an HP1100 system equipped with a diode array detector using a Vydac C_{18} reversed-phase semipreparative column.

1.2.2: RU COMPLEX SYNTHESIS

Dipyrido[3,2-*a*:2′,3′-*c*]phenazine (dppz) and 4′-methyl-2,2′-bipyridine-4-carboxylic acid (mcbpy) were prepared according to previously recorded procedures.[18,19] 4-Aminomethyl-4′-methyl-2,2′-bipyridine (NH_2-bpy) was prepared from 4,4′-dimethyl-2,2′-bipyridine as described by Berg et al. (to make 4-hydroxymethyl-4′-methyl-2,2′-bipyridine) and Hamachi et al.[20,21]

1.2.2.1: SYNTHESIS OF 4-ETHOXY-4′-METHYL-2,2′-BIPYRIDINE (CO_2ET-BPY)

4′-methyl-2,2′-bipyridine-4-carboxylic acid (111 mg) was refluxed in 10 mL ethanol with conc. H_2SO_4 (10 drops). Reaction progress was complete by 8 h, as monitored by TLC (silica, 5% methanol in CH_2Cl_2). The mixture was cooled to 0 °C and neutralized with saturated $NaHCO_3$, then concentrated *in vacuo*. Water was added, and the solution was extracted with CH_2Cl_2. The organic layer was washed with water, dried with Na_2SO_4, filtered, and concentrated *in vacuo*. The pale yellow solid was purified on a silica column using 1:1 ethyl acetate:hexanes to yield a white solid. ^{1}H NMR (acetone-d_6, 300 MHz): δ 8.98 (m, 1H), 8.86 (dd, 1 H, 5.0 Hz, 1.1 Hz), 8.57 (m, 1H), 8.34 (m, 1H), 7.89 (dd, 1 H, 5.0 Hz, 1.7 Hz), 7.30 (dd, 1 H, 5.0 Hz, 1.1 Hz), 4.45 (q, 2H, 7.1 Hz), 2.47 (s, 3H), 1.42 (t, 3H, 7.1 Hz).

1.2.2.2: SYNTHESIS OF 4-NH-FMOC-4′-METHYL -2,2′-BIPYRIDINE

4-Aminomethyl-4′-methyl-2,2′-bipyridine (45 mg, 0.23 mmol) was dissolved in 3 mL CH_2Cl_2. 9-Fluorenylmethoxy-carbonyl-N-hydroxysuccinimide (Fmoc-OSu) (114 mg, 0.34 mmol), dissolved in 3 mL CH_2Cl_2, was added. After 2 h, 59 μL DIEA was added, and the mixture was stirred under $Ar_{(g)}$ for 29 h. The solution was rinsed twice with saturated sodium bicarbonate. The dichloromethane solution was dried with magnesium sulfate, filtered, and concentrated *in vacuo*. The product was purified by silica column (pre-treated with 90:10 hexanes:triethylamine), eluting with 1:1 ethyl acetate:hexanes followed by ethyl acetate. A white solid was obtained. ESI-MS (cation): 422.2 *m/z* ($M^+ + H^+$) obsd, 422.2 *m/z* ($M^+ + H^+$) calcd. ^{1}H NMR ($CDCl_3$, 300 MHz):

δ 8.62 (d, 1H, 5.1 Hz), 8.53 (d, 1H, 5.1 Hz), 8.30 (s, 1H), 8.23 (s, 1 H), 7.77 (d, 2H, 7.5 Hz), 7.61 (d, 2H, 7.5 Hz), 7.41 (m, 2H), 7.31 (m, 2H), 7.19 (d, 1H, 5.1 Hz), 7.15 (d, 1H, 3.6 Hz), 5,23 (broad s, 1H), 4.49 (m, 4H), 4.25 (t, 1H, 6.6 Hz), 2.45 (s, 3 H).

1.2.2.3: SYNTHESIS OF $[RuL_2DPPZ]Cl_2$; L = 2,2′-BIPYRIDINE (BPY), 1,10-PHENANTHROLINE (PHEN), OR 4,7-DIPHENYL-1,10-PHENATHROLINE (DIP)

$Ru(bpy)_2Cl_2$ was synthesized as previously described.[22] $Ru(DIP)_2Cl_2$ and $Ru(phen)_2Cl_2$ were synthesized in an analogous fashion to $Ru(bpy)_2Cl_2$. The dipyridophenazine (dppz) ligand was added to RuL_2Cl_2 by refluxing in ethanol-water for > 3 h to make $Ru(DIP)_2dppz^{2+}$ and $Ru(phen)_2dppz^{2+}$. The ethanol was removed under vacuum, resulting in precipitation of $[Ru(DIP)_2dppz]Cl_2$, which was collected by filtration. The compound was purified via room temperature recrystallization by diffusion of ether into acetonitrile. $Ru(phen)_2dppz^{2+}$ was precipitated from water as the hexafluorophosphate salt, then returned to the chloride salt by Sephadex DEAE anion exchange column. The Ru complexes utilized are racemic mixtures of the two enantiomers. Ru complex concentrations were determined by UV/vis absorbance: $Ru(bpy)_2dppz^{2+}$, $\varepsilon_{444\ nm}$ = 16,100 M^{-1} cm^{-1};[24] $Ru(phen)_2dppz^{2+}$, $\varepsilon_{440\ nm}$ = 21,100 M^{-1} cm^{-1};[25] and $Ru(DIP)_2dppz^{2+}$, $\varepsilon_{433\ nm}$ = 34,300 M^{-1} cm^{-1}.

1.2.2.4: SYNTHESIS OF $[Ru(Me_4phen)_2dppz]Cl_2$

$Ru(Me_4phen)_2Cl_2$ was synthesized in a similar manner to $Ru(bpy)_2Cl_2$, except that the reaction time was shortened to 3 h (reaction for 8 h produces a larger amount of

impurities), and the reaction was performed under $Ar_{(g)}$ and protected from light. Dppz was added to $Ru(Me_4phen)_2Cl_2$ as described above to form $Ru(Me_4phen)_2dppz^{2+}$. The complex, as the PF_6^- salt, was first purified on a neutral alumina column, eluting with CH_3CN. The product was converted to the Cl^- salt by anion exchange chromatography (Sephadex DEAE). Further purification by HPLC yielded the complex in analytical purity. ESI-MS (cation): 428.2 *m/z* (M^{2+}) obsd, 428.1 *m/z* (M^{2+}) calcd. UV/vis (H_2O, pH 5): 269 nm (130,500 M^{-1} cm^{-1}), 358 nm (18,100 M^{-1} cm^{-1}), 376 nm (22,900 M^{-1} cm^{-1}), 422 nm (21,200 M^{-1} cm^{-1}).

1.2.2.5: SYNTHESIS OF $[Ru(CO_2Et\text{-}bpy)_2dppz]Cl_2$

$Ru(CO_2Et\text{-}bpy)_2Cl_2$ was synthesized according to the protocol of Leasure and coworkers,[23] except 2:1 dimethoxyethane:ethanol was used as the reaction solvent. The dppz ligand was added by refluxing in ethanol for 24 h. The complex was purified by a neutral alumina column eluting with CH_3CN, followed by recrystallization by slow diffusion of ether into CH_3CN. Complex was converted to the Cl^- salt by anion exchange chromatography (Sephadex DEAE). ESI-MS (cation): 433.9 *m/z* (M^{2+}) obsd, 434.1 *m/z* (M^{2+}) calcd. UV/Vis (H_2O, pH 5): 293 nm (110,000 M^{-1} cm^{-1}), 360 nm (28,700 M^{-1} cm^{-1}), 372 nm (28,200 M^{-1} cm^{-1}), 463 nm (29,300 M^{-1} cm^{-1}).

1.2.2.6: SYNTHESIS OF $Ru(mcbpy)_2dppz$

This complex was formed by hydrolysis of the ester. $[Ru(CO_2Et\text{-}bpy)_2dppz]Cl_2$ was suspended in 0.5 M LiOH and stirred overnight. The reaction mixture was

neutralized with 1 M HCl and desalted with a Sep-Pak C_{18} cartridge (Waters Chemical Co). A red-orange solid was obtained. ESI-MS (cation): 406.0 *m/z* (MH_2^{2+}), 416.9 *m/z* ($MNaH^{2+}$), 427.9 *m/z* (MNa_2^{2+}) obsd, 406.1 *m/z* (MH_2^{2+}) calcd. UV/Vis (H_2O, pH 5): 292 nm (100,200 M^{-1} cm^{-1}), 358 nm (25,400 M^{-1} cm^{-1}), 372 nm (24,600 M^{-1} cm^{-1}), 458 nm (25,400 M^{-1} cm^{-1}).

1.2.2.7: SYNTHESIS OF $[RU(NH_2\text{-}BPY)_2DPPZ]CL_2$

This complex was synthesized using the Fmoc-protected ligand, 4-NH-Fmoc-4′-methyl-2,2′-bipyridine. Preparation of $Ru(NH\text{-}Fmoc\text{-}bpy)_2Cl_2$ was accomplished using the method of Leasure and coworkers.[23] Dppz was added by refluxing in 1:1 ethanol:water for 7 h. The ethanol was removed *in vacuo*, and the water solution was filtered. $Ru(NH\text{-}Fmoc\text{-}bpy)_2dppz^{2+}$ was precipitated by addition of NH_4PF_6 to the filtrate, and converted to the chloride salt by anion exchange chromatography (Sephadex DEAE). Product was purified by HPLC.

Deprotection of $Ru(NH\text{-}Fmoc\text{-}bpy)_2dppz^{2+}$ to give $Ru(NH_2\text{-}bpy)_2dppz^{2+}$ was performed using 0.5% piperidine (v/v) in DMF for 15 min. Higher concentrations of piperidine (5%) produced impurities. The DMF/piperidine solution was removed *in vacuo*. The residue was dissolved in water, filtered, and the product was precipitated as the PF_6^- salt using NH_4PF_6. After rinsing carefully with water, the orange solid was dissolved in 1:1 acetonitrile:water and converted to the chloride salt by anion exchange chromatography (Sephadex DEAE). ESI-MS (cation): 391.1 *m/z* (M^{2+}) obsd, 391.1 *m/z*

(M^{2+}) calcd. UV/Vis (H_2O, pH 5): 286 nm (99,400 M^{-1} cm^{-1}), 359 nm (19,900 M^{-1} cm^{-1}), 371 nm (19,500 M^{-1} cm^{-1}), 458 nm (17,900 M^{-1} cm^{-1}).

1.2.3: CELL CULTURE

Cell lines were maintained in the following medium: minimal essential medium alpha with 10% fetal bovine serum (FBS), 100 units/mL penicillin, and 100 μg/mL streptomycin for HeLa (ATCC, CCL-2) and DU-145 (ATCC, HTB-81); McCoy's 5a medium with 10% FBS, 100 units/mL penicillin, and 100 μg/mL streptomycin for SKOV-3 (ATCC, HTB-77) and HT-29 (ATCC, HTB-38**)**; F-12K medium with 10% FBS 100 units/mL penicillin, and 100 μg/mL streptomycin for A-549 (ATCC, CCL-185); and RPMI medium 1640 supplemented with 10% FBS, 2 mM L-glutamine, 0.1 mM nonessential amino acids, 1 mM sodium pyruvate, 100 units/mL penicillin, 100 μg/mL streptomycin, and 400 μg/mL Geneticin (G418) for HCT116N and HCT116O. Cells were grown in tissue culture flasks at 37 °C under 5% CO_2 atmosphere.

1.2.4: FLOW CYTOMETRY

Cells were detached from culture with EDTA (0.48 mM in phosphate-buffered saline) and incubated at $1x10^6$ cells/mL with 10 μM ruthenium complex (added from a concentrated stock) in Hanks' Balanced Salt Solution (HBSS) supplemented with 2.5 mg/mL bovine serum albumin fraction V (BSAV) at 37 °C for 2 h, then rinsed with buffer and placed on ice. TO-PRO-3 was added at 1 μM immediately prior to flow cytometry analysis to stain dead cells. The fluorescence of ~20,000 cells was measured

using a BD FACS Aria at the Caltech Flow Cytometry Facility. Ruthenium complexes were excited at 488 nm, with emission observed at 600–620 nm. TO-PRO-3 was excited at 633 nm, with emission observed at 650–670nm. Cells exhibiting TO-PRO-3 fluorescence were excluded from the data analysis. For nuclei experiments, the nuclei buffer (vide infra) was used as the sheath fluid on the flow cytometer.

1.2.5: CONFOCAL MICROSCOPY

Cells used for microscopy were seeded on glass-bottom 96-well plates (Whatman) and allowed to attach overnight. For incubations shorter than 24 h, approximately 4000 cells were seeded. Longer incubations required that fewer cells be seeded to allow room for cell proliferation, e.g., for the cell line comparison experiments, 3000 cells were seeded. After incubation with the ruthenium complex in complete medium (containing 10% fetal bovine serum), cells were rinsed with Hanks' Balanced Salt Solution and imaged without fixation (unless otherwise noted). Images were collected on a Zeiss LSM 510 or Zeiss LSM 5 Exciter inverted microscope using a 63x/1.4 oil immersion objective at the Caltech Biological Imaging Center. Nuclei were examined using a 20x objective. The ruthenium complexes were excited at 488 nm, with emission observed using a long-pass 560 nm filter.

For the cell fixation experiments, HeLa cells were incubated with 5 μM $Ru(DIP)_2dppz^{2+}$ for 2 h at 37 °C. One well of cells was subsequently treated with cold methanol for ~ 3 min and rinsed with phosphate-buffered saline (PBS). A second well

was fixed with 2% formaldehyde for 5 min, then permeabilized with 0.1% Triton X-100 in PBS for 6 min.

1.2.6: ISOLATION OF NUCLEI

Cells were detached with trypsin (no EDTA) for 5 min at 37 °C. The cells were rinsed once with cold phosphate-buffered saline (PBS), then resuspended in cold nuclei extraction buffer (320 mM sucrose, 5 mM $MgCl_2$, 10 mM HEPES, 1% Triton X-100 at pH 7.4), giving approximately 1 mL per 1 million cells. The cell suspension was vortexed for 10 s and incubated on ice for 9 min. The nuclei were pelleted by centrifuged at 2000 g (~2950 rpm) for 4 min at 4 °C, washed twice with cold nuclei wash buffer (320 mM sucrose, $MgCl_2$, 10 mM HEPES at pH 7.4), and resuspended in cold nuclei wash buffer with vortexing. The solution was triturated 5–10 times with a 1 mL micropipette to break up clumps of nuclei, then filtered through a 35 μm cell strainer (BD Falcon) to remove any remaining clumps. The nuclei solution was stored on ice until analysis. Nuclei isolation was confirmed by examining an aliquot mixed with an equal volume of 0.4% Trypan blue (the nuclei stain blue). For confocal microscopy, nuclei were suspended in PBS prior to imaging.

The following control for contamination of nuclei by ruthenium during the lysis procedure was performed. The cell lysates from cells incubated with ruthenium complex were filtered through 0.2 μm nylon membrane (Whatman Centrex MF-5.0 filters), by centrifugation at 1,700–2,000 rpm. HeLa that were not incubated with ruthenium were detached with trypsin (no EDTA) and rinsed once with cold PBS. The cells were

resuspended in cold cell lysate (from the Ru-treated cells), vortexed, and incubated on ice for 9 min. The nuclei were pelleted by centrifugation at 2000 g (2,950 rpm) for 4 min at 4 °C, then washed twice with cold nuclei wash buffer. The nuclei were resuspended in cold nuclei wash buffer, vortexed, and triturated to break up clumps. The solution was filtered through a 35 μm cell strainer and stored on ice until analysis.

1.3: RESULTS AND DISCUSSION

1.3.1: STRATEGY TO MEASURE UPTAKE

The dipyridophenazine (dppz) complexes of ruthenium(II) act as reporters for non-aqueous environments, luminescing only when bound to the hydrophobic regions of membranes, nucleic acids, and other macromolecules.[26,27] Using their luminescence as a handle, we can readily analyze their cellular accumulation by confocal microscopy and flow cytometry.

Ru(II) polypyridyl complexes provide a systematic route for comparing factors affecting uptake, since ligands can be easily varied with respect to their characteristics and then metalated via the same synthetic strategy. In addition, the complexes under study are coordinatively saturated, with ligands that are inert to substitution. As a result, they are stable in buffer, medium, and the cellular environment. Their characteristic luminescence indicates that the complexes remain intact once inside the cell, as any decomposition or loss of ligands, albeit unlikely, would render the complexes non-luminescent.

A series of Ru(II) dppz complexes was synthesized for evaluation of their cellular uptake properties. Substituting the ancillary ligands on the dppz complex permits variation in the overall complex charge, size, and hydrophobicity (**Figure 1.1**).

1.3.2: CHARACTERISTICS OF THE RUTHENIUM COMPLEXES

Since the nature of the ancillary ligands can affect the luminescence properties of the ruthenium complexes, we measured their relative luminescence in CH_3CN and when bound to calf thymus DNA (**Table 1.1**). The complexes were excited at 488 nm, the same wavelength used for the confocal microscopy and flow cytometry experiments. The integrated emissions at 600–620 nm and 560–800 nm, the ranges recorded in flow cytometry and confocal microscopy analysis, respectively, are compared. All the complexes are non-luminescent in aqueous solution, but display luminescence in CH_3CN and in the presence of DNA. Also, there is no evidence of non-specific protein binding giving luminescence. Notably, $Ru(DIP)_2dppz^{2+}$ exhibits enhanced emission compared to the other complexes.

The lipophilicity of a compound can have a large influence on its cellular uptake. A common measure of a compound's lipophilicity is its octanol-water partition coefficient (*P*), defined as the ratio of the equilibrium concentrations of the dissolved compound in 1-octanol and water. This value is usually given in the form of its logarithm to base 10 (log *P*). Measurement of the partition coefficient can be performed by the "shake-flask" method or by HPLC analysis in comparison to reference substances.[28] We include the partition coefficients of our ruthenium complexes, obtained by the

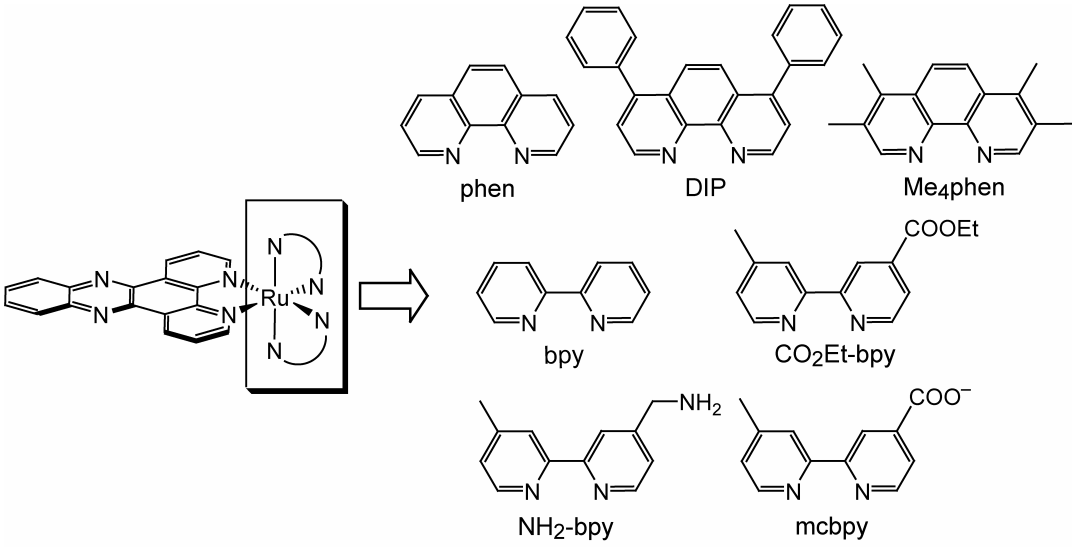

Figure 1.1: Dipyridophenazine complexes of Ru(II).

Table 1.1: Characteristics of the Ru complexes

ancillary ligand of RuL_2dppz	relative emission intensity in CH_3CN[a] 600–620 nm	relative emission intensity w/DNA[a,b] 600–620 nm	relative emission intensity in CH_3CN[a] 560–800 nm	relative emission intensity w/DNA[a,b] 560–800 nm	octanol/H_2O partition coefficient (log *P*)[c]	diameter (Å)[d]
bpy	1.0	1.0	1.0	1.0	-2.50	16.2
CO_2Et-bpy	1.8	1.1	2.2	1.4	-0.76	20.4
mcbpy	1.2	0.6	1.7	0.6	-0.43	18.2
NH_2-bpy	0.6	1.6	0.9	1.6	n.d.	17.8
phen	1.2	2.3	1.2	2.0	-1.48	16.2
Me_4phen	0.2	0.3	0.4	0.4	-0.79	17.4
DIP	2.7	2.7	2.6	2.4	1.30	20.4

[a]Excited at 488 nm; integrated emission over the indicated range. 10 μM Ru was used, except for $Ru(DIP)_2dppz^{2+}$ in Tris buffer, where a lower concentration was used due to poor solubility; emission values were scaled accordingly. [b]Luminescence values with DNA were obtained at saturation. [c]Cl^- salt. [d]Diameters were estimated using Titan. Data not determined are indicated by n.d.

shake-flask method, in **Table 1.1**. The only complex to prefer the octanol phase to water is $Ru(DIP)_2dppz^{2+}$.

Another factor that may affect a compound's uptake profile is its size. The diameters of our ruthenium complexes were estimated using the program Titan, and these are listed in **Table 1.1**. The largest complexes are $Ru(DIP)_2dppz^{2+}$ and $Ru(CO_2Et\text{-}bpy)_2dppz^{2+}$ at approximately 20.4 Å in diameter, and the smallest complexes are $Ru(phen)_2dppz^{2+}$ and $Ru(bpy)_2dppz^{2+}$ at 16.2 Å in diameter.

1.3.3: FLOW CYTOMETRY ANALYSIS OF UPTAKE

Flow cytometry allows the rapid quantification of luminescence intensity of individual cells as they pass single file through the laser beam, with thousands of cells analyzed in a few minutes. For our studies, we employed TO-PRO-3, a membrane impermeable dye, to stain dead cells and exclude them from analysis. The resulting data for the cell population can be displayed as a histogram of luminescence intensity versus number of cells. Uptake for different ruthenium complexes may be compared using the mean luminescence intensity of the cell population.

We used flow cytometry to examine the effect of ancillary ligand variation on the accumulation of dipyridophenazine complexes of Ru(II) in the human cervical cancer cell line, HeLa. Cells were incubated with 10 μM RuL_2dppz (where L = bpy, phen, NH_2-bpy, CO_2Et-bpy, mcbpy, Me_4phen, and DIP) for 2 h at 37 °C. The mean luminescence intensity of cells exposed to $Ru(DIP)_2dppz^{2+}$ ranges from 11-fold to 47-fold greater than that of the other complexes, and this difference is too large to be due solely to the

superior brightness of $Ru(DIP)_2dppz^{2+}$ (**Figure 1.2**, **Table 1.2**). The lipophilic DIP ligand seems to facilitate uptake, despite the larger size of the complex. Consistent with its intermediate lipophilicity, $Ru(Me_4phen)_2dppz^{2+}$ exhibits less efficient uptake than $Ru(DIP)_2dppz^{2+}$, but still better than the other complexes. $Ru(phen)_2dppz^{2+}$, $Ru(bpy)_2dppz^{2+}$, $Ru(NH_2\text{-}bpy)_2dppz^{4+}$, and $Ru(CO_2Et\text{-}bpy)_2dppz^{2+}$ are taken up to some extent, but little luminescence is evident for $Ru(mcbpy)_2dppz$. The lower emission intensity of $Ru(mcbpy)_2dppz$ with nucleic acids contributes to its relatively poor luminescence inside cells but cannot fully account for it. Likely, its reduced overall charge impairs its ability to use the membrane potential as a driving force for cellular entry (see Chapter 2). Accordingly, $Ru(NH_2\text{-}bpy)_2dppz^{4+}$, with its increased positive charge, exhibits slightly better uptake than $Ru(bpy)_2dppz^{2+}$.

These results are in agreement with uptake studies on cisplatin analogues, where the complexes with the greatest lipophilicity exhibit the highest uptake. Although, for the Pt complexes, all were hydrophilic, with octanol-water partition coefficients of < 1.[12]

1.3.4: CONFOCAL MICROSCOPY IMAGING

1.3.4.1: UPTAKE AND LOCALIZATION OF THE RU COMPLEXES

The subcellular distribution of our dipyridophenazine complexes of Ru(II) was studied using confocal microscopy. $Ru(DIP)_2dppz^{2+}$, which exhibits the greatest uptake by flow cytometry analysis, accumulates predominantly in the cytoplasm of HeLa cells. Luminescence is evident in the cell interior within 2 h when incubated at 5 μM (**Figure 1.3A**). Under similar conditions (10 μM, 2 h), $Ru(Me_4phen)_2dppz^{2+}$ is observed

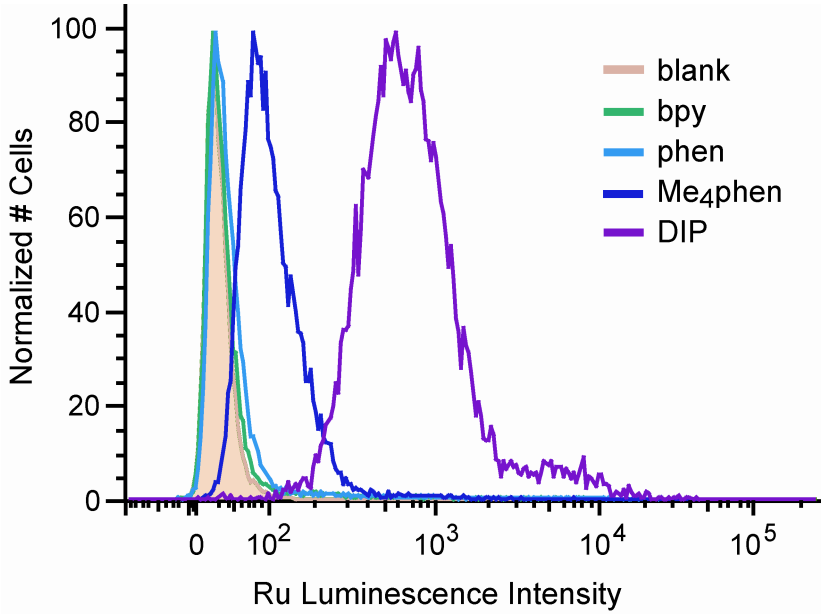

Figure 1.2: Flow cytometry analysis of ruthenium complex cellular uptake. HeLa cells were incubated with 10 μM RuL_2dppz^{2+} (where L = bpy, phen, Me_4phen, and DIP) for 2 h at 37 °C. Luminescence data were obtained by excitation at 488 nm with emission at 600–620 nm. Dead cells were excluded from analysis using the membrane impermeable dye TO-PRO-3.

Table 1.2: Cellular uptake of ruthenium complexes assayed by flow cytometry

ancillary ligand of RuL_2dppz	mean luminescence[a]
bpy	39 ± 2
NH_2-bpy	56 ± 4
CO_2Et-bpy	68 ± 4
mcbpy	25 ± 1
phen	79 ± 17
Me_4phen	107 ± 1
DIP	1169 ± 87

[a]HeLa cells were incubated with 10 μM ruthenium complex for 2 h at 37 °C. Ruthenium complexes were excited at 488 nm, with emission observed at 600–620 nm. The mean luminescence intensity of cells not treated with complex is 20. Each data point is the mean ± the standard deviation of three samples.

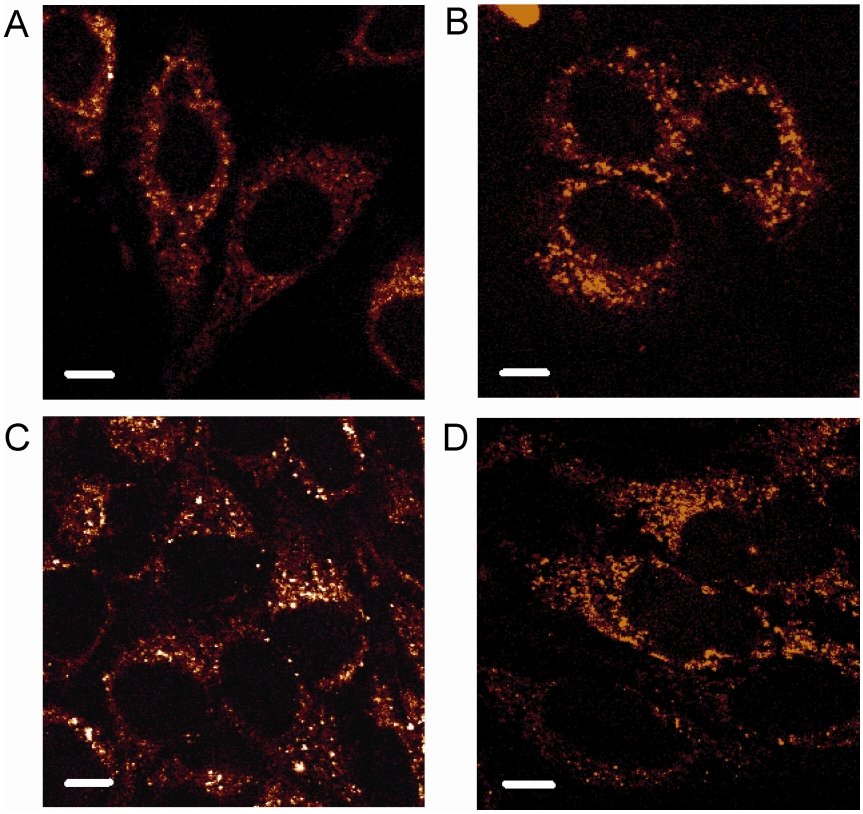

Figure 1.3: Confocal microscopy of HeLa cells incubated with dipyridophenazine complexes of Ru(II). (A) $Ru(DIP)_2dppz^{2+}$ (5 μM, 2 h).

(B) $Ru(Me_4phen)_2dppz^{2+}$ (10 μM, 2 h). (C) $Ru(phen)_2dppz^{2+}$ (20 μM, 24 h).

(D) $Ru(bpy)_2dppz^{2+}$(20 μM,72 h). Scale bars are 10 μm.

inside the cytoplasm of cells (**Figure 1.3B**). All of the other complexes, including $Ru(bpy)_2dppz^{2+}$ and $Ru(phen)_2dppz^{2+}$, which display limited uptake at 10 μM and 2 h by flow cytometry analysis, are also internalized, though longer incubation times and/or higher concentrations are required to obtain high-quality confocal images (**Figures 1.3C, 1.3D**). Inside the cell, the complexes are likely protected from water by macromolecular binding, without which quenching in the cytosol is expected.

At a slightly higher concentration and longer incubation time (10 μM, 12 h), there is a small increase in the amount of $Ru(DIP)_2dppz^{2+}$ in the nucleus, as shown by line plot quantitation (**Figure 1.4**), though the majority of complex remains in the cytoplasm. Longer incubations (5 μM, 72 h) do not produce a preference for the nucleus.

For most of the complexes, their exact location in the cytoplasm is difficult to discern. However, for $Ru(bpy)_2dppz^{2+}$, some of the luminescence has a stringy appearance that is characteristic of mitochondria (**Figure 1.5**). The putative mitochondrial staining is less intense than the additional, globular staining; as a result, it is visible in many but not all cells.

1.2.4.2: LIVE VERSUS FIXED CELL IMAGING

Cell fixation can sometimes alter the subcellular distribution of compounds. For example, some peptide-fluorophore conjugates have been shown to move from the cytoplasm to the nucleus following fixation with formaldehyde.[16] We evaluated the effect of different fixation methods on the localization of $Ru(DIP)_2dppz^{2+}$.

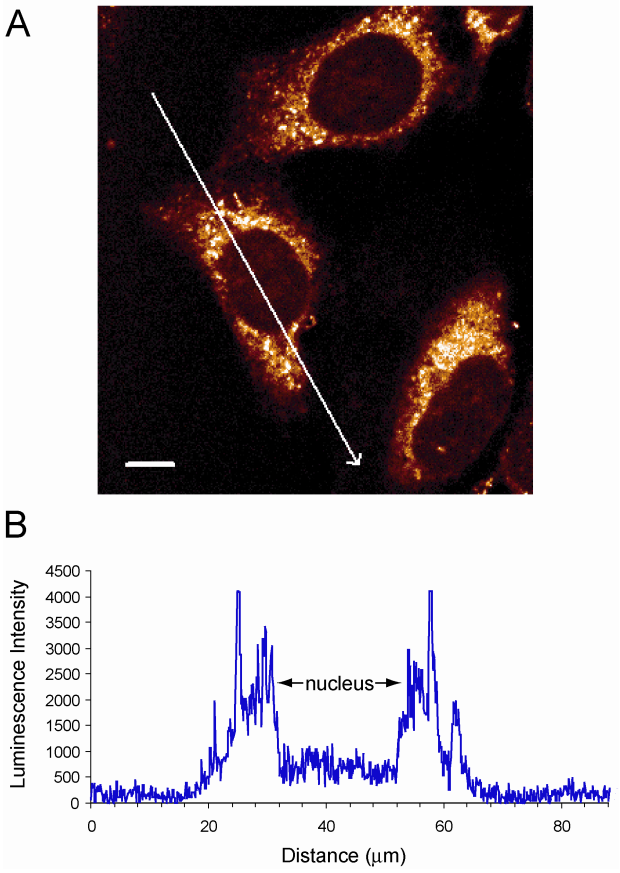

Figure 1.4: Quantitation of nuclear uptake. (A) HeLa cells were incubated for 12 h with 10 μM $Ru(DIP)_2dppz^{2+}$. Scale bar is 10 μm. The arrow indicates the section taken for the line plot in (B).

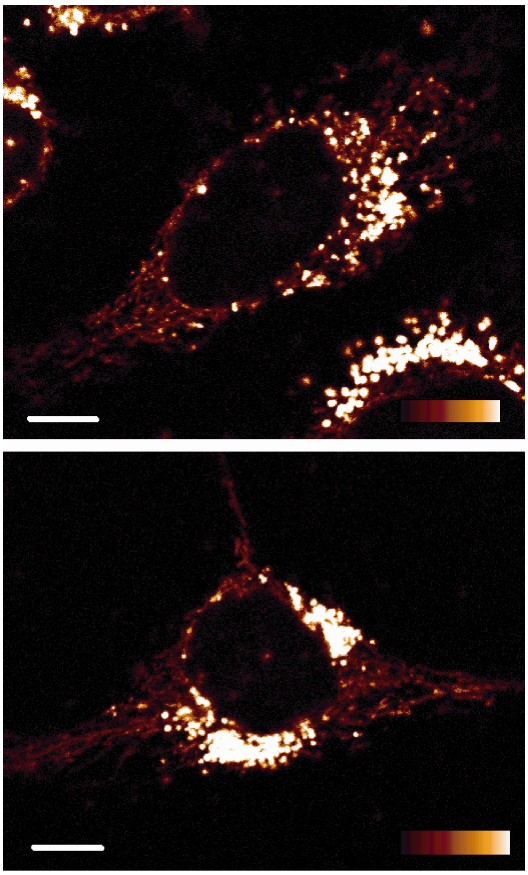

Figure 1.5: Subcellular localization of $Ru(bpy)_2dppz^{2+}$. HeLa cells were incubated with 40 μM $Ru(bpy)_2dppz^{2+}$ for 24 h. Scale bars (white) are 10 μm. The luminescence is shown on an intensity scale, denoted by the color-coded scale bars.

Live HeLa cells, incubated with 5 μM $Ru(DIP)_2dppz^{2+}$ for 2 h, were imaged before fixation to reveal cytoplasmic staining. Treatment with cold methanol causes a dramatic redistribution of the complex almost entirely to the nucleus (**Figure 1.6**). Though methanol enhances the luminescence of these complexes, the cells were rinsed with buffer following fixation and only trace methanol should remain. Likely, methanol solubilizes $Ru(DIP)_2dppz^{2+}$, aiding its diffusion into the now more permeable nucleus. Once inside the nucleus, the complex can bind to DNA, resulting in intense luminescence. In contrast, fixation with 2% formaldehyde does not produce any noticeable changes in the subcellular distribution of $Ru(DIP)_2dppz^{2+}$. Permeabilization of the formaldehyde-treated cells with 0.1% Triton X-100 (a non-ionic detergent), however, results in some nuclear accumulation of the complex. Rinsing with buffer following Triton X-100 treatment did not abrogate this effect, indicating that the increased luminescence is not conferred directly by presence of the fixative.

Formaldehyde appears to have fewer effects on ruthenium complex localization than methanol. Nevertheless, all of the confocal microscopy studies described elsewhere in this thesis were performed on live cells.

1.3.5: ANALYSIS OF ISOLATED NUCLEI

The metal complexes of the Barton lab target DNA, therefore we are keenly interested in the ability of our complexes to accumulate inside the nucleus. Hence, flow cytometry analysis of isolated nuclei was performed. In contrast to the live cell experiments, we cannot discriminate nuclei originating from dead cells versus those from

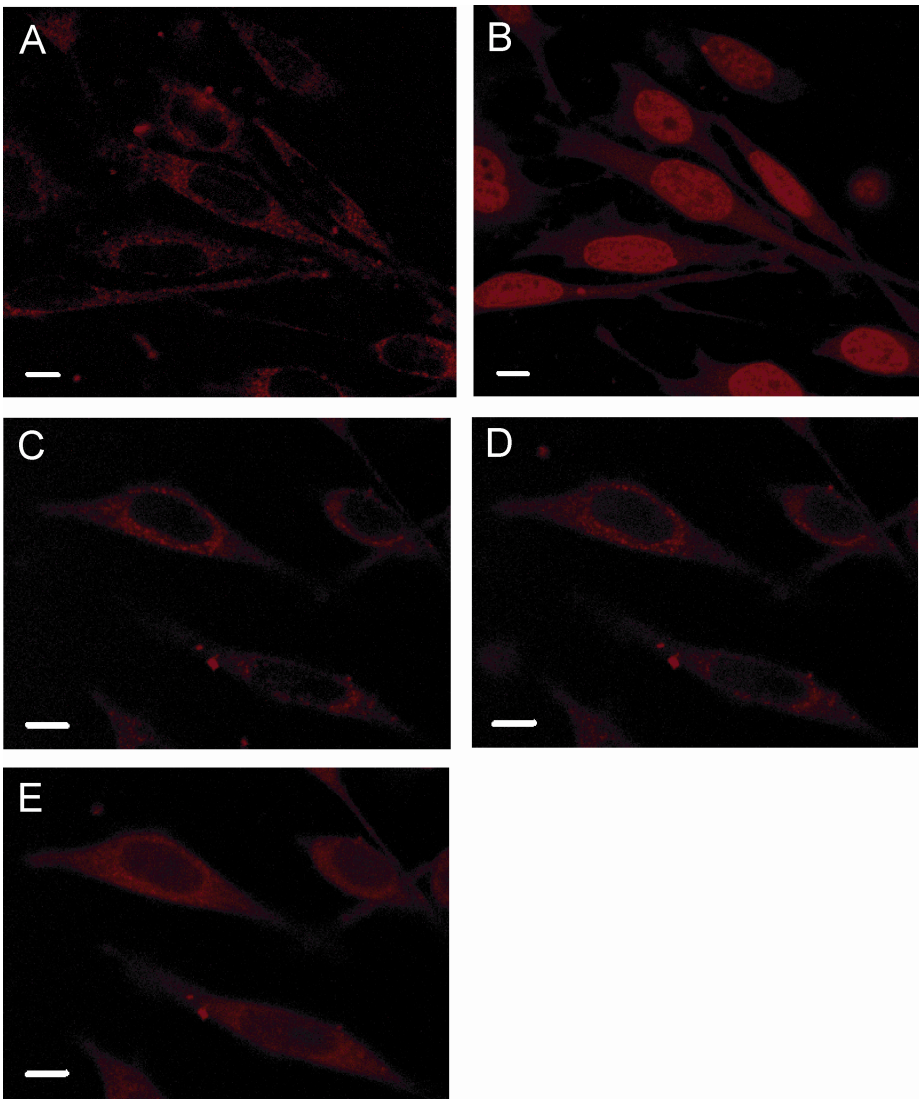

Figure 1.6: Effect of fixation on ruthenium complex subcellular localization. HeLa cells were incubated with 5 μM $Ru(DIP)_2dppz^{2+}$ for 2 h. Live cells (A, C) show cytoplasmic localization. After fixation of Ru-treated cells with methanol (B), the ruthenium complex relocates almost entirely to the nucleus. Fixation with 2% formaldehyde does not change the distribution (D), but treatment of the formaldehyde-fixed cells with 0.1% Triton X-100 increases the nuclear staining (E). Scale bars are 10 μm.

live cells. However, we expect that dead cells would accumulate a much greater amount of complex, resulting in nuclei that can be recognized by their increased staining. Also, analogous to the whole cell experiments, complex bound to the exterior of the nucleus cannot be distinguished from that in the interior. Therefore, confocal microscopy must be used to confirm internalization.

Nuclei isolated from HeLa cells incubated with 5 or 10 μM $Ru(DIP)_2dppz^{2+}$ for 2 h at 37 °C were analyzed for Ru uptake by flow cytometry. The mean luminescence intensity of the nuclei population increased substantially compared to nuclei from cells not treated with complex (**Figure 1.7**), consistent with nuclear uptake. Two populations of nuclei are seen in the histogram, with the population at very high luminescence likely coming from dead cells. Nuclei from cells incubated with 10 μM complex show greater luminescence than those incubated with 5 μM complex. There is also a positive correlation between length of incubation (2–24 h) and intensity of the ruthenium luminescence.

In order to isolate the nuclei, the cells are lysed. Since this procedure also permeabilizes the nuclear envelope, there is a possibility that during cell lysis, ruthenium complex located in the cytoplasm could move into the nucleus. Thus, we performed the following control for contamination of nuclei by ruthenium during the lysis procedure. Cells, which had not been incubated with ruthenium complex, were lysed using cell lysate from cells incubated with complex. These nuclei showed similar luminescence as the untreated, autofluorescence controls, which indicates that no substantial crossover of

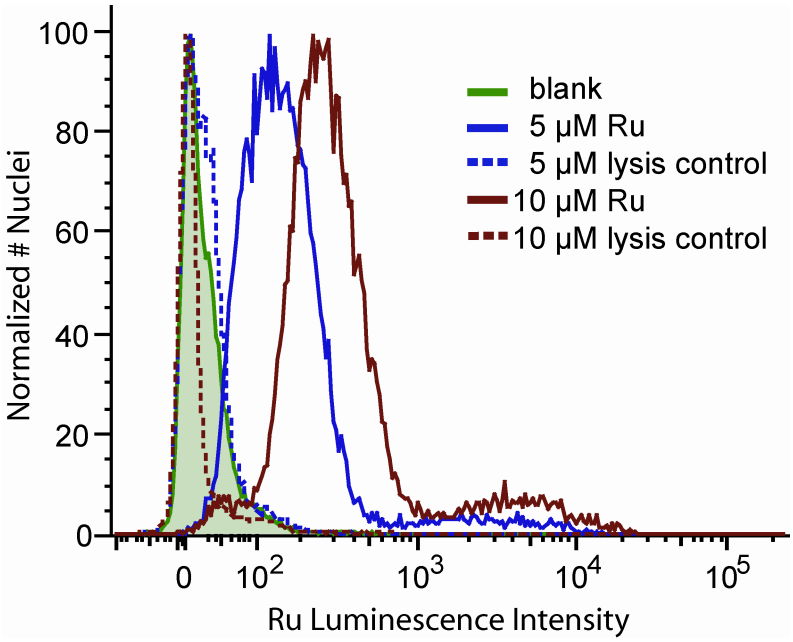

Figure 1.7: Flow cytometry analysis of nuclei isolated from HeLa cells incubated with 5 or 10 µM $Ru(DIP)_2dppz^{2+}$ for 2 h at 37 °C. Controls were performed to evaluate the extent of Ru contamination into the nucleus from the cytoplasm during lysis. For these controls, cells were lysed using cell lysate from cells incubated with $Ru(DIP)_2dppz^{2+}$.

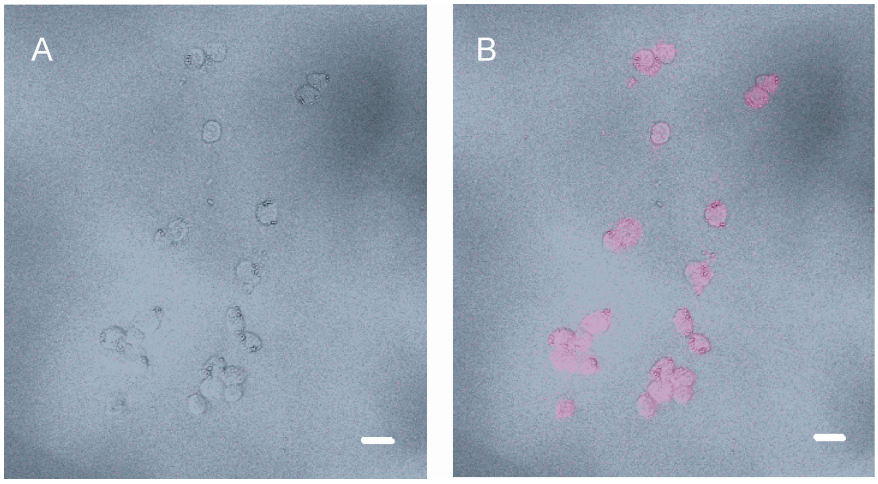

Figure 1.8: Confocal microscopy of nuclei isolated from HeLa cells incubated with 5 µM $Ru(DIP)_2dppz^{2+}$ for 2 h at 37 °C. (A) 1.1 µm optical slice. (B) 10.0 µm optical slice, which encompasses the entire thickness of the nuclei. Images are shown as overlay of the transmitted light image (gray) and the ruthenium luminescence (red). Scale bars are 20 µm.

ruthenium complex from the cytoplasm to the nucleus occurs during lysis.

Nuclei isolated from HeLa incubated with 5 μM $Ru(DIP)_2dppz^{2+}$ for 2 h at 37 °C were also examined by confocal microscopy (**Figure 1.8**). Ruthenium luminescence is not visible when the optical slice is set to 1.1 μm. When the optical slice is widened to 10.0 μm, thus increasing the sensitivity, the nuclei are brightly luminescent, which is consistent with the flow cytometry data. Ruthenium complex is associated with the nucleus, but the presence inside the nucleus cannot be established based on the 10.0 μm optical slice, because it encompasses the entire thickness of the nucleus.

Although we cannot confirm nuclear uptake using confocal microscopy of isolated nuclei when cells are treated with 5 μM $Ru(DIP)_2dppz^{2+}$, we can observe some complex inside the nucleus of intact cells when the incubation concentration is increased to 10 μM for 12 h (vide supra). Presumably, nuclei isolated from such cells would also show nuclear uptake. Furthermore, the increased luminescence of nuclei from treated versus untreated cells, the concentration dependence, and the time dependence observed by flow cytometry are all consistent with nuclear accumulation.

1.3.6: CELL LINE COMPARISON

The cellular accumulation and subcellular distribution of a compound can vary dramatically between cell types. For example, Dervan and co-workers have observed different degrees of nuclear uptake of pyrrole-imidazole polyamides depending on the cell line.[29] Hence, we compare the cellular uptake of our dipyridophenazine complexes of Ru(II) in human cancer cell lines derived from several different tissue types, namely

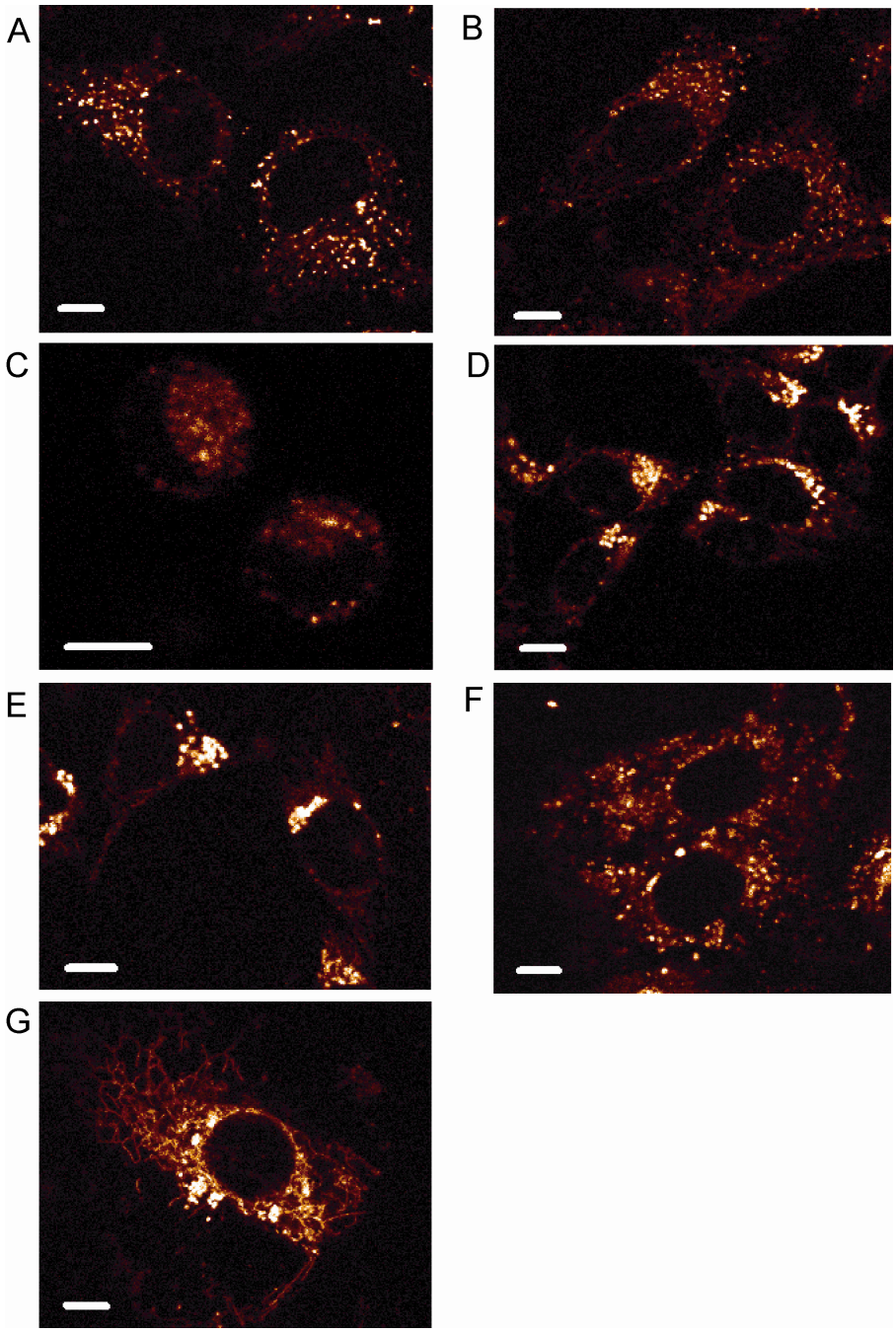

Figure 1.9: Accumulation of $Ru(bpy)_2dppz^{2+}$ by different cell lines. $Ru(bpy)_2dppz^{2+}$ (40 μM, 24 h) was incubated with (A) HeLa, (B) SKOV-3, (C) HT-29, (D) HCT116N, (E) HCT116O, (F) A-549, and (G) DU-145. Scale bars are 10 μm.

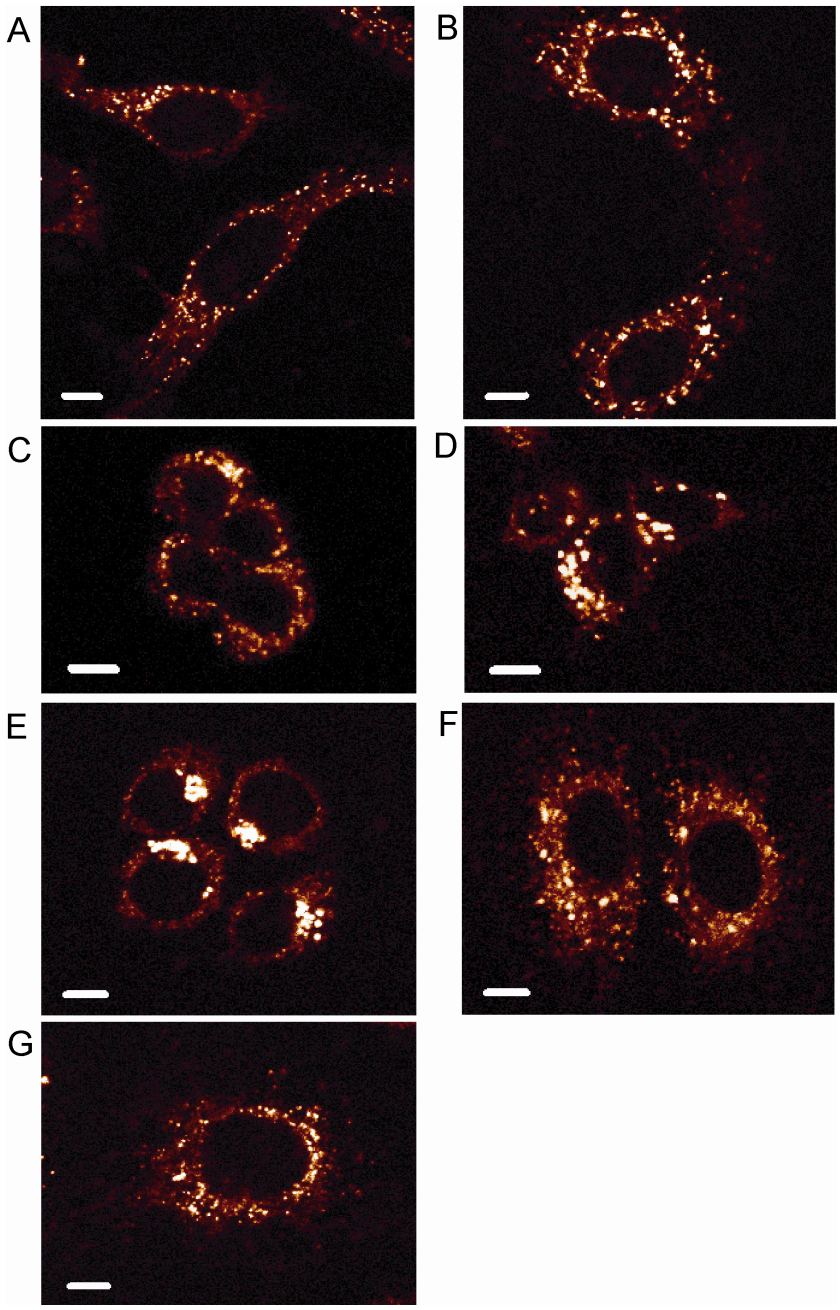

Figure 1.10: Accumulation of $Ru(phen)_2dppz^{2+}$ by different cell lines.

$Ru(phen)_2dppz^{2+}$ (40 μM, 24 h) was incubated with (A) HeLa, (B) SKOV-3, (C) HT-29, (D) HCT116N, (E) HCT116O, (F) A-549, and (G) DU-145. Scale bars are 10 μm.

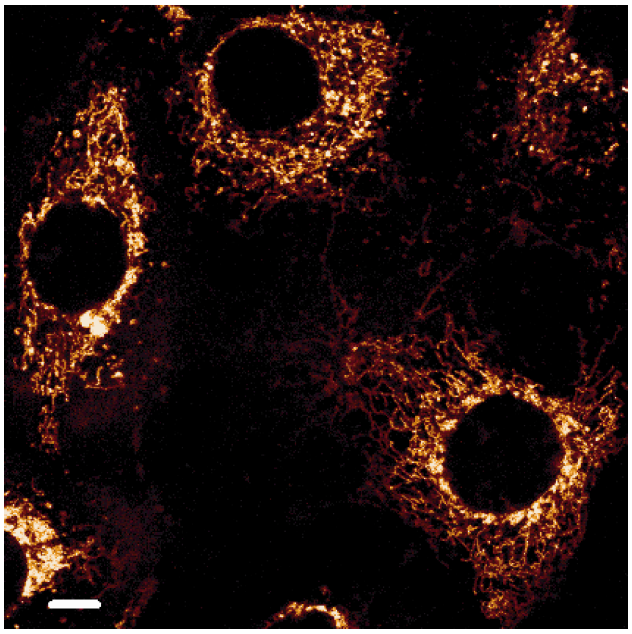

Figure 1.11: Accumulation of $Ru(bpy)_2dppz^{2+}$ in DU-145 cells. $Ru(bpy)_2dppz^{2+}$ was incubated at 40 μM for 24 h. The morphology of the staining is characteristic of mitochondria. Scale bar is 10 μm.

HeLa (cervix), SKOV-3 (ovary), HT-29 (colon), HCT116O (colon), HCT116N (colon), DU-145 (prostate), and A-549 (lung).

The cells, seeded at identical density, were incubated with 40 μM $Ru(bpy)_2dppz^{2+}$ or 40 μM $Ru(phen)_2dppz^{2+}$ in complete medium for 24 h then rinsed with buffer and imaged by confocal microscopy. Instrument settings were kept the same to allow for direct comparison of the luminescence intensity between the cell lines.

In all of the cell lines, both $Ru(bpy)_2dppz^{2+}$ and $Ru(phen)_2dppz^{2+}$ were localized in the cytoplasm but were absent from the nucleus (**Figures 1.9, 1.10**). The appearance of the cytoplasmic staining was similar between the lines, except for DU-145, where $Ru(bpy)_2dppz^{2+}$ seems to accumulate preferentially in mitochondria. Here, the staining displays a stringy shape that is characteristic of mitochondria (**Figures 1.9G, 1.11**). This pattern is also seen in HeLa treated with $Ru(bpy)_2dppz^{2+}$, but in a smaller percentage of the cells along with additional non-mitochondrial staining (**Figures 1.5, 1.9A**). Since the complex carries a positive charge, it may be pulled into the mitochondria in response to the membrane potential. However, the reason that mitochondrial localization is preferred by one cell line more than the others is not clear.

1.4: CONCLUSIONS

Using a series of dipyridophenazine complexes of Ru(II), we systematically compared the factors affecting cellular uptake and distribution. We find that $Ru(DIP)_2dppz^{2+}$ exhibits enhanced cellular accumulation compared to other complexes studied. Uptake appears to be facilitated by the lipophilic DIP ligand, even at the cost of

expanded size. Accordingly, $Ru(Me_4phen)_2dppz^{2+}$, which is intermediate in lipophilicity between $Ru(DIP)_2dppz^{2+}$ and $Ru(phen)_2dppz^{2+}$, enters cells with efficiency less than $Ru(DIP)_2dppz^{2+}$ but better than $Ru(phen)_2dppz^{2+}$. Reducing the charge of the complex hinders uptake: little luminescence is apparent for the neutral complex, $Ru(mcbpy)_2dppz$. In contrast, increasing charge from +2 to +4 results in a modest increase in uptake: luminescence of $Ru(NH_2\text{-}bpy)_2dppz^{4+}$ is slightly greater than that of $Ru(bpy)_2dppz^{2+}$. This correlation between charge and uptake is consistent with the plasma membrane potential serving as the driving force for cellular entry.

The complexes accumulate in the cytoplasm of live cells but are mostly excluded from the nucleus. However, flow cytometry analysis of nuclei isolated from cells treated with $Ru(DIP)_2dppz^{2+}$ are consistent with some nuclear entry, and nuclear staining is apparent by confocal microscopy when the incubation concentration is sufficiently high (10 μM, 12 h). Importantly, the rhodium analogues that we are exploring as potential therapeutic agents have been demonstrated to exert their biological effect in a manner dependent on direct binding to DNA,[6] implying that these complexes reach the nucleus. The present studies suggest that the population responsible for activity represents a fraction of the total compound inside the cell.

Ruthenium luminescence in the cytoplasm is uneven, which could indicate association with organelles, though the exact subcellular localization is not clear. This staining pattern is consistent across several different human cancer cell lines, with two exceptions. For HeLa and DU-145 cells incubated with $Ru(bpy)_2dppz^{2+}$, the morphology of the staining pattern is characteristic to that of mitochondria (**Figures 1.5, 1.11**).

Furthermore, we demonstrate that confocal microscopy and flow cytometry, in concert, are effective techniques for characterizing internalization and distribution of luminescent transition metal complexes. Ruthenium analogues in particular can be readily tested without special instrumentation or complicated synthesis; they can be excited by the 488-nm laser, common to most confocal microscopy and flow cytometry systems. Statistics on thousands of cells of varied cell type, under different incubation conditions, and using a range of metal complexes can be generated to provide a powerful complement in the design of metal complexes for biological application.

These data establish that the ruthenium complexes indeed accumulate in human cancer cell lines isolated from a variety of tissue types. In the following chapters, we will explore the mechanism of uptake and strategies to direct the compounds to the nucleus.

1.5: REFERENCES

1. Bruijnincx, P. C. A.; Sadler, P. J. *Curr. Opin. Chem. Biol.* **2008,** *12,* 197–206.
2. Jakupec, M. A.; Galanski, M.; Arion, V. B.; Hartinger, C. G.; Keppler, B. H. *Dalton Trans.* **2008,** 183–194.
3. Montgomery, C. P.; Murray, B. S.; New, E. J.; Pal, R.; Parker, D. *Acc. Chem. Res.* **2009,** *42,* 925–937.
4. Hart, J. R.; Glebov, O.; Ernst, R. J.; Kirsch, I. R.; Barton, J. K. *Proc. Natl. Acad. Sci. U. S. A.* **2006,** *103*, 15359–15363.
5. Zeglis, B. M; Pierre, V. C.; Barton, J. K. *Chem. Commun.* **2007**, 4565–4579.
6. Ernst, R. J.; Song, H.; Barton, J. K. *J. Am. Chem. Soc.* **2009,** *131,* 2359–2366.
7. Lipinski, C. A.; Lombardo, F.; Dominy, B. W.; Feeney, P. J. *Adv. Drug Delivery Rev.* **2001,** *46,* 3–26.
8. Hall, M. D.; Okabe, M.; Shen, D. W.; Liang, X. J.; Gottesman, M. M. *Annu. Rev. Pharmacol. Toxicol.* **2008,** *48,* 495–535.
9. New, E. J.; Parker, D. *Org. Biomol. Chem.* **2009,** *7,* 851–855.
10. Jiménez-Hernández, M. E.; Orellana, G.; Montero, F.; Portolés, M. T. *Photochem. Photobiol.*, **2000,** *72,* 28–34.
11. Egger, A. E.; Rappel, C.; Jakupec, M. A.; Hartinger, C. G.; Heffeter, P.; Keppler, B. K. *J. Anal. At. Spectrom.* **2009,** *24,* 51–61.
12. Ghezzi, A.; Aceto, M.; Cassino, C.; Gabano E.; Osella, D. *J. Inorg. Biochem.* **2004,** *98,* 73–78.

13. Kirin, S. I.; Ott, I.; Gust, R.; Mier, W.; Weyhermüller, T.; Metzler-Nolte, N. *Angew. Chem. Int. Ed.* **2008,** *47,* 955–959.

14. Jonas, S. K.; Riley, P. A. *Cell Biochem. Funct.* **1991,** *9,* 245–253.

15. Davies, D.; C. Hughes, C. Dead cell discrimination. In *In Living Color: Protocols in Flow Cytometry and Cell Sorting,* 1st ed.; Diamond, R. A., DeMaggio, S., Eds.; Springer: Berlin, 2000.

16. Richard, J. P.; Melikov, K.; Vives, E.; Ramos, C.; Verbeure, B.; Gait, M. J.; Chernomordik, L. V.; Lebleu, B. *J. Biol. Chem.* **2003,** *278,* 585–590.

17. Hällbrink, M.; Oehlke, J.; Papsdorf, G.; Bienert, M. *Biochim. Biophys. Acta* **2004,** *1667,* 222–228.

18. Dickeson, J. E.; Summers, L. A. *Aust. J. Chem.* **1970,** *23,* 1023–1027.

19. McCafferty, D. G.; Bishop, B. M.; Wall, C. G.; Hughes, S. G.; Mecklenberg, S. L.; Meyer, T. J.; Erickson, B. W. *Tetrahedron* **1995,** *51,* 1093–1106.

20. Berg, K. E.; Tran, A; Raymond, M. K.; Abrahamsson, M.; Wolny, J.; Redon, S.; Andersson, M.; Sun, L. C.; Styring, S.; Hammarström, L.; Toftlund, H.; Åkermark, B. *Eur. J. Inorg. Chem.* **2001,** 1019–1029.

21. Hamachi, I.; Tanaka, S.; Tsukiji, S.; Shinkai, S.; Oishi, S. *Inorg. Chem.* **1998,** *37,* 4380–4388.

22. Sullivan, B. P.; Salmon, D. J.; Meyer, T. J. *Inorg. Chem.* **1978,** *17*, 3334–3341.

23. Leasure, R. M.; Ou, W.; Moss, J. A.; Linton, R. W.; Meyer, T. J. *Chem. Mater.* **1996,** *8,* 264–273.

24. Chambron, J.-C.; Sauvage, J.-P. *Chem. Phys. Lett.* **1991,** *182,* 603–607.

25. Holmlin, R. E.; Stemp, E. D. A.; Barton, J. K. *Inorg. Chem.* **1998,** *37*, 29–34.

26. Friedman, A. E.; Chambron, J.-C.; Sauvage, J.-P.; Turro, N. J.; Barton, J. K. *J. Am. Chem. Soc.* **1990,** *112,* 4960–4962.

27. Jenkins, Y.; Friedman, A. E.; Turro, N. J.; Barton, J. K. *Biochemistry* **1992,** *31,* 10809–10816.

28. Sangster, J. Experimental Methods of Measurement. *Octanol-Water Partition Coefficients: Fundamentals and Physical Chemistry;* John Wiley & Sons: Chichester, U.K., 1997.

29. Edelson, B.; Best, T.; Olenyuk, B.; Nickols, N. Doss, R.; Foister, S.; Heckel, A.; Dervan, P. *Nucleic Acids Res.* **2004,** *32,* 2802–2818.